ELSEVIER

International Journal of Mass Spectrometry 223–224 (2003) 473–489

International Journal of Mass Spectrometry

www.elsevier.com/locate/ijms

Stark mixing in Rydberg atoms by ultralow energy collisions with ions

M.R. Flannery*, D. Vrinceanu

School of Physics, Georgia Institute of Technology, Atlanta, GA 30332, USA

Received 4 February 2002; accepted 24 May 2002

Abstract

Quantal and classical theories developed recently for the full array of $n\ell \rightarrow n\ell'$ transitions (Stark mixing) in Rydberg atoms by collision with slow ions are summarized. Quantal and classical probabilities $P^{(n)}_{\ell'\ell}$ are provided for transitions in atomic hydrogen, induced by the time-dependent (dipole) electric field generated by adiabatic collision with charged particles. A universal classical scaling law permits examination of the (rapid) convergence of the quantal probabilities onto the classical background as n is increased. The structure exhibited in the variation of $P^{(n)}_{\ell'\ell}$ with ℓ' is explained and a quantal–classical correspondence is manifest. A modification to take account of quantum defects in Rydberg systems (with quantum defects) is presented. Essential agreement is obtained with measurements of Na^+–Na(28d) collisions. (Int J Mass Spectrom 223–224 (2003) 473–489)

PACS: 34.50.Pi; 34.60.+z; 34.10.+x

Keywords: Stark mixing; Rydberg atoms; Collision

1. Introduction

The ion-Rydberg atom/molecule collisional process

$$A^{Z+} + Ry(n, \ell) \rightarrow A^{Z+} + Ry(n, \ell') \quad (1)$$

is called collisional Stark mixing since the ℓ-changing transitions $\ell \rightarrow \ell'$ occur within the same energy shell n of the Rydberg species and are induced by the time-dependent electric field generated by the passing ion A^{Z+}. The process is significant over a broad range of interest and applications. For example, the formation of anti-hydrogen by three-body recombination $e^+ + \bar{p} + e^+ \rightarrow \bar{H} + e^+$ at ultralow energies, where the sequence [1] is collisional capture into high $\ell \rightarrow$ states, followed by Stark mixing collisions $n\ell \rightarrow n\ell'$ and by radiative relaxation. Since the n-changing collisions are relatively unimportant at ultralow energies, the ℓ-mixing collisions are essential in producing the low angular momentum states required to radiatively decay at relatively high rate to low n-levels, thereby stabilizing the recombination. In zero-kinetic-energy-photo-electron spectroscopy (ZEKE-PES), high ℓ states are produced [2] from low ℓ states by electric fields. It is also significant in dissociative recombination [3–5]. Experiments [6] on Na^+–Na(28d) collisions have measured large ℓ-mixing cross-sections, even for dipole-forbidden transitions.

The process is also interesting from a theoretical point of view and has remained largely unsolved for

* Corresponding author.

1387-3806/02/$ – see front matter
PII S1387-3806(02)00931-4

four decades. Notable historical landmarks include a modified first-order impact parameter treatment [7], a classical diffusion theory [8], hydrogen atom in weak E–B fields [9], a truncated closely-coupled channel system of equations [10], Monte-Carlo simulations [11], and quantal and classical treatments of $0 \to \ell'$ transitions [12–15].

Exact solutions of Stark mixing in atomic hydrogen induced by the time-dependent (dipole) electric field generated by (adiabatic) collision with a slow ion and probabilities for the full array $n\ell \to n\ell'$ of transitions were only recently presented [16–19] in both classical and quantal formulations. The exceptionally rich dynamical symmetry of the hydrogen atom provides the key foundation which enables both the classical [16,17] and quantal solutions [17–19] to be constructed in a unified way, by using group representation theory. In this paper (dedicated to Werner Lindinger), a full case study of collisional Stark mixing is presented, together with exploration of classical–quantal convergence and correspondence for the full transition array.

2. Group symmetry

Conserved quantities for Coulomb attraction are the unperturbed Hamiltonian

$$H_0 = \frac{p^2}{2m_e} - \frac{e^2}{r},$$

the angular momentum $\boldsymbol{L} = \boldsymbol{r} \times \boldsymbol{p}$ and also the classical Runge–Lenz vector

$$\boldsymbol{A} = p_n^{-1}\left[\boldsymbol{p} \times \boldsymbol{L} - m_e e^2 \frac{\boldsymbol{r}}{r}\right],$$

directed toward the pericenter and normalized to angular momentum units, are all conserved. The operator $\boldsymbol{A}$ has the symmetrized (Pauli–Lenz) quantal form

$$\boldsymbol{A} = \frac{1/2(\boldsymbol{p} \times \boldsymbol{L} - \boldsymbol{L} \times \boldsymbol{p}) - m_e e^2 \hat{r}}{p_n}$$

where $p_n = (-2m_e E_n)^{1/2}$ and the eigenenergy $E_n = -(1/2n^2)(e^2/a_0)$. Components of $\boldsymbol{A}$ satisfy the following relationships:

$$\begin{aligned}
&[A_j, H] = 0 && \text{: i.e., } \boldsymbol{A} \text{ is a conserved quantity,}\\
&[L_j, A_k] = i\hbar\epsilon_{jkn}A_n && \text{: i.e., } \boldsymbol{A} \text{ is also a system vector,}\\
&[A_j, A_k] = i\hbar\epsilon_{jkn}L_n && \text{: i.e., } \boldsymbol{A}\text{'s components do not commute,}\\
&\boldsymbol{A}\cdot\boldsymbol{L} = \boldsymbol{L}\cdot\boldsymbol{A} = 0 && \text{: i.e., the vector } \boldsymbol{A} \text{ is orthogonal on } \boldsymbol{L},\\
&A^2 + L^2 = (n^2-1)\hbar^2 && \text{: i.e., } A \text{ is constant for intrashell transitions,}
\end{aligned}$$

where ϵ_{kjn} is the Levi–Civita antisymmetric symbol for any $k, j = 1, 2, 3$. Hence $(E_n, \boldsymbol{L}, \boldsymbol{A})$ provide five independent conserved quantities. These commutation relations define the SO(4) dynamic symmetry group for the restricted motion of the orbital electron to the energy shell. The SO(4) operators can be disentangled by introducing $\boldsymbol{J}_\pm = (\boldsymbol{L} \pm \boldsymbol{A})/2$. Each $\boldsymbol{J}_+$ and $\boldsymbol{J}_-$ operator separately generates a SO(3) subalgebra, such that $\mathrm{SO}(4) \equiv \mathrm{SO}(3) \oplus \mathrm{SO}(3)$. The $\boldsymbol{J}_\pm$ operators therefore commute i.e., $[\boldsymbol{J}_+, \boldsymbol{J}_-] = 0$, obey usual angular momentum rules $[J_j, J_k] = i\hbar\epsilon_{jkn}J_n$ and have integral or half-integral eigenvalues $J_\pm^2 = j(j+1)\hbar^2$ where $j = (n-1)/2$. In classical treatments, the quantum operators $\boldsymbol{L}$ and $\boldsymbol{A}$ are replaced by their classical vectors and the quantal commutators $(i\hbar)^{-1}[B, C]$ by the corresponding Poisson brackets. The classical analogy is that the set of coupled equations for $\boldsymbol{L}$ and $\boldsymbol{A}$ in a constant electric field $\boldsymbol{\mathcal{E}}$ become decomposed into an uncoupled set for the vectors $\boldsymbol{J}_\pm$ which independently precess [20] with Stark frequency $\boldsymbol{\omega}_S = (3e/2p_n)\boldsymbol{\mathcal{E}}$ about the electric field direction $\boldsymbol{\mathcal{E}}$ according to

$$\frac{\mathrm{d}\boldsymbol{J}_\pm}{\mathrm{d}t} = \pm\boldsymbol{\omega}_S \times \boldsymbol{J}_\pm. \tag{2}$$

3. Collision interaction

Fig. 1 illustrates the collision dynamics. The frequencies of the Rydberg electron and the collision are $\omega_n = v_n/a_n$ and $\omega_R = |\dot{\Phi}|$, respectively. Here $a_n = n^2 a_0$ and $v_n = p_n/m_e = v_0/n$ are the orbital

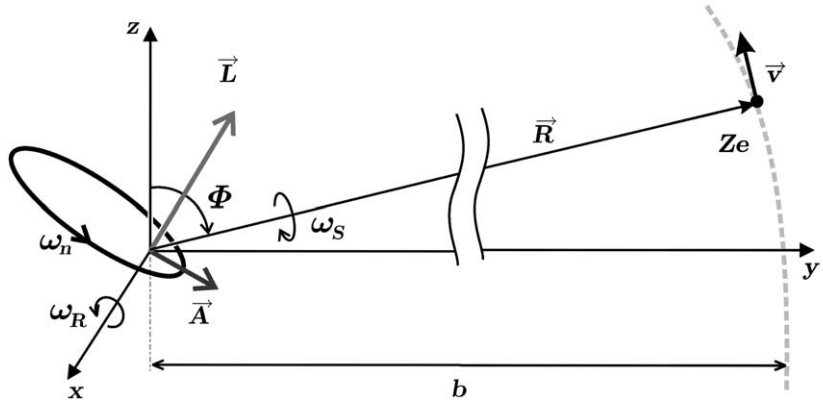

Fig. 1. Ion-Rydberg collision dynamics and the characteristic frequencies ω_n (orbital), ω_R (collisional) and ω_S (Stark).

radius and velocity, averaged so that $e^2/a_n = p_n v_n$. For slow variation of the electric field $\boldsymbol{\mathcal{E}}$, generated by the passing ion, our simulation of the collision in Fig. 2 shows that the frequencies are ordered as $\omega_S < \omega_R < \omega_n$. It also shows that, although $\boldsymbol{L}$ and $\boldsymbol{A}$ change little during one orbit, significant change is accomplished during the collision over the course of many (∼50) electron orbits. It also indicates that the ℓ-changing collision at ultralow impact energies satisfies the following three approximations:

3.1. Orbital adiabatic

This means that the collision is much slower than the much more rapid motion of the orbital Rydberg electron. The collision frequency $\omega_R \ll$, the orbital frequency ω_n of the Rydberg electron. In classical treatments, the electron position vector $\boldsymbol{r}$ can then be replaced by its average $\langle \boldsymbol{r} \rangle = -(3/2p_n)\boldsymbol{A}$. For quantal matrix elements within the same energy shell,

$$\langle n\ell' m' | \boldsymbol{r} | n\ell m \rangle = -\left(\frac{3}{2p_n}\right) \langle n\ell' m' | \boldsymbol{A} | n\ell m \rangle \tag{3}$$

which is Pauli's replacement rule [21]. The collision is orbital adiabatic in the region $b > (v/v_n)a_n$.

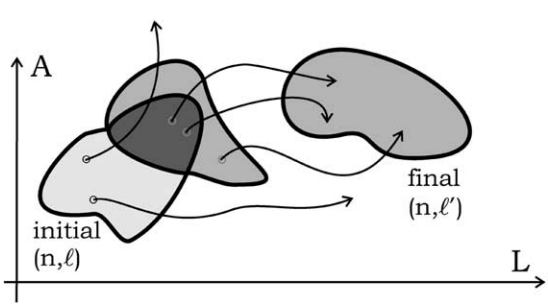

Fig. 2. The classical probability is a ratio of the two phase space volumes: the volume of the region within that part of the initial-state manifold containing coordinates which can evolve into the final state manifold, and the total volume of the initial-state manifold.

3.2. Weak field

Collisions which change only angular momentum occur at large impact parameters b where the ion-Rydberg atom interaction potential is the ion–dipole potential $V = -\boldsymbol{d} \cdot \boldsymbol{\mathcal{E}}$, where $\boldsymbol{d} = -e\boldsymbol{r}$ is the dipole strength and where the electric field $\boldsymbol{\mathcal{E}} = -Ze\hat{\boldsymbol{R}}/R^2$ is constant over the spatial extent of the atom. The Stark frequency is then

$$\omega_S = \frac{3e}{2p_n}\boldsymbol{\mathcal{E}} = -\left(\frac{3Ze^2}{2p_n R^2}\right)\hat{\boldsymbol{R}}$$

Under these adiabatic and dipole assumptions, interaction with the electric field is then characterized by

$$V(\boldsymbol{A}, \boldsymbol{R}) = -\boldsymbol{d} \cdot \boldsymbol{\mathcal{E}} = -\omega_S(\boldsymbol{R}) \cdot \boldsymbol{A}. \tag{4}$$

The weak field region is where the Stark energy splitting $\hbar\omega_S \ll \hbar\omega_n$, the separation between neighboring

energy levels, i.e., the region $b \approx R \gg (3Z/2)^{1/2}a_n$ where the dipole assumption is valid.

3.3. Classical path

Since the angular momentum $\mu R^2\dot{\Phi}$ of relative motion of the heavy-particle collision system of reduced mass μ is very much greater than the angular momentum $\ell\hbar$ of the Rydberg electron, it is conserved to $-\mu v b$ so that $R^{-2} = -\dot{\Phi}/bv$.

Under the dipole and classical path assumptions, the Stark frequency is

$$\boldsymbol{\omega}_{\mathrm{S}} = \frac{3e}{2p_n}\boldsymbol{\mathcal{E}} = (\alpha\dot{\Phi})\hat{\boldsymbol{R}} \tag{5}$$

where the dimensionless Stark parameter is defined as the ratio

$$\alpha = \frac{\omega_{\mathrm{S}}}{\omega_{\mathrm{R}}} = \frac{3Z}{2}\left(\frac{a_n v_n}{bv}\right) = \frac{3Z}{2}\left(\frac{a_n}{b}\right)^2\left(\frac{\tau_{\mathrm{coll}}}{\tau_0}\right) \tag{6}$$

of Stark to collision frequencies. Also $\tau_{\mathrm{coll}} = b/v$ is a measure of the collision duration and $\tau_0 = a_0/v_0$ is the au of time. The ion–hydrogen adiabatic interaction is then

$$\begin{aligned} V(\boldsymbol{A}, \Phi; \alpha) &= -\boldsymbol{\omega}_{\mathrm{S}} \cdot \boldsymbol{A} \\ &= -\alpha\frac{\mathrm{d}\Phi}{\mathrm{d}t}(A_2 \sin\Phi + A_3 \cos\Phi) \end{aligned} \tag{7}$$

which has the advantage that it is expressed only in terms of the generators of the SO(4) group. Moreover, the components $\{L_1, A_2, A_3\}$ generate a subgroup of the original symmetry group. Under the above three approximations, the resulting set of quantal and classical equations governing the problem of collisional Stark mixing at ultralow energies can be solved exactly.

4. Quantal theory

4.1. Quantal intrashell dynamics

The Schrödinger equation for the time evolution operator $U(t, t_0)$ is

$$i\hbar\frac{\partial U}{\partial t} = (H_0 + V)U \tag{8}$$

where H_0 is the free atom Hamiltonian and V is the interaction potential. In the interaction representation, the corresponding equation is

$$i\hbar\frac{\partial U_I}{\partial t} = V_I U_I \tag{9}$$

where $V_I = \mathrm{e}^{iH_0 t/\hbar} V \mathrm{e}^{-iH_0 t/\hbar}$ and $U_I(t, t_0) = \exp(iH_0 t/\hbar)U(t, t_0)\exp(-iH_0 t_0/\hbar)$ are the corresponding potential and evolution operators in the interaction representation. The transition probability for a general $i \to f$ transition at time t is

$$\begin{aligned} a_{fi}(t) &= \langle\Phi_f(\boldsymbol{r}, t)|\Psi_i(\boldsymbol{r}, t)\rangle \\ &\equiv \langle\Phi_f(\boldsymbol{r}, t)|U(t, t_0)|\Phi_i(\boldsymbol{r}, t_0)\rangle \\ &= \langle\phi_f(\boldsymbol{r})|U_I(t, t_0)|\phi_f(\boldsymbol{r})\rangle \end{aligned} \tag{10}$$

where Ψ_i is the target wavefunction under external interaction V. In the asymptotic limits ($t \to \pm\infty$), it tends to the unperturbed basis set $\Phi_j(\boldsymbol{r}, t) = \phi_j(\boldsymbol{r})\exp(-iE_j t/\hbar)$. The transition amplitude for a Stark mixing process is $a_{\beta\alpha}^{(n)} = \langle n\beta|U_I(\infty, -\infty)|n\alpha\rangle$ where α and β now label the states within the same energy shell. The potential matrix elements $\langle n\beta|V_I(t)|n\alpha\rangle = \langle n\beta|V(t)|n\alpha\rangle$ are then identical. The superscript n will now be omitted, since all dynamics is restricted to the energy shell described by quantum number n. Eq. (9) with $V_I = V$ is then

$$\begin{aligned} i\hbar\frac{\partial U_I}{\partial\Phi} &= -\alpha(A_2 \sin\Phi + A_3 \cos\Phi)U_I \\ &= -\alpha\left(\mathrm{e}^{i\Phi L_1/\hbar}A_3\,\mathrm{e}^{-i\Phi L_1/\hbar}\right)U_I \end{aligned} \tag{11}$$

in which the basic identity

$$\mathrm{e}^{\lambda A}B\,\mathrm{e}^{-\lambda A} = B + \frac{\lambda}{1!}[A, B] + \frac{\lambda^2}{2!}[A, [A, B]] + \cdots \tag{12}$$

and the commutation relation $[L_j, A_k] = i\hbar\epsilon_{jkn}A_n$ above are invoked. The exact solution of (11) is

$$\begin{aligned} U_I(t, t_0) = \mathrm{e}^{i\Phi L_1/\hbar}\exp\left[-\frac{i}{\hbar}\Delta\Phi(L_1 - \alpha A_3)\right] \\ \times\,\mathrm{e}^{-i\Phi_0 L_1/\hbar} \end{aligned} \tag{13}$$

This can also be directly verified from (11) with use of the appropriate commutator algebra. The

probabilities for full array of Stark mixing transition $\ell \to \ell'$ transitions can be obtained from

$$P^{(n)}_{\ell'\ell} = \frac{1}{2\ell+1} \sum_{m=-\ell}^{\ell} \sum_{m'=-\ell'}^{\ell'} |\langle n\beta|U_I(\infty,-\infty)|n\alpha\rangle|^2 \tag{14}$$

The direct use of (15) permitted analytical probabilities [17,18] to be obtained only for low $n = 2, 3$. Numerical calculations were required for higher n. However, upon the decomposition $\boldsymbol{L} = \boldsymbol{M} + \boldsymbol{N}$ and $\boldsymbol{A} = \boldsymbol{M} - \boldsymbol{N}$, the solution separates as

$$U_I = U_M \otimes U_N$$

where the operators U_M and U_N are defined by

$$U_M = \mathrm{e}^{i\Phi M_1/\hbar}\, \mathrm{e}^{-i\Delta\Phi(M_1-\alpha M_3)/\hbar}\, \mathrm{e}^{-i\Phi_0 M_1/\hbar}$$

and

$$U_N = \mathrm{e}^{i\Phi N_1/\hbar}\, \mathrm{e}^{-i\Delta\Phi(N_1+\alpha N_3)/\hbar}\, \mathrm{e}^{-i\Phi_0 N_1/\hbar}$$

and where $\Delta\Phi(t) = \Phi(t) - \Phi(t_0)$ is the polar angle swept out by $\boldsymbol{R}$ within time interval $(t - t_0)$. Since the angular momentum-like operators $\boldsymbol{M}$ and $\boldsymbol{N}$ commute, the corresponding evolution operators U_M and U_N act independently as rotations in carrier spaces of dimension $2j + 1 = n$. The probability for transition $\ell \to \ell'$ between states with given angular momentum is defined by

$$P^{(n)}_{\ell'\ell} = \frac{1}{2\ell+1} \sum_{m=-\ell}^{\ell} \sum_{m'=-\ell'}^{\ell'} \left| a^{(n)}_{\ell' m' \leftarrow \ell m} \right|^2 \tag{15}$$

where the $(\ell, m) \to (\ell', m')$ transition amplitude between angular momentum states within the energy shell of quantum number n is

$$a^{(n)}_{\ell' m' \leftarrow \ell m} = \langle n\ell' m'|U_M \otimes U_N|n\ell m\rangle = \sum_{\mu\nu\mu'\nu'} C^{\ell m}_{j\mu j\nu} C^{\ell' m'}_{j\mu' j\nu'} \mathcal{D}^{(j)}_{\mu'\mu}(U_M) \mathcal{D}^{(j)}_{\nu'\nu}(U_N) \tag{16}$$

and where $\mathcal{D}^{(j)}(R)$ is Wigner's $2j + 1$ dimensional matrix representation of the finite rotation R.

4.2. Quantal transition probability: exact solution

The 10 folded summation within the quantal probability (15) has been contracted [19] to yield the following compact form,

$$P^{(n)}_{\ell'\ell}(\chi) = \frac{2\ell'+1}{n} \sum_{L=|\ell'-\ell|}^{n-1} (2L+1) \times \begin{Bmatrix} \ell' & \ell & L \\ j & j & j \end{Bmatrix}^2 H^2_{jL}(\chi) \tag{17}$$

for the transition $\ell \to \ell'$ probability between any states with given angular momentum. This involves only one summation. Here $\{\cdots\}$ is the $6-j$ symbol for coupling of three angular momenta, $j = (n-1)/2$ and H_{jL} is a special matrix element of the irreducible representation of the group O(4). This function (also called the generalized character χ^j_L, associated with the irreducible representation of the rotation group) is well studied (see, for example, the books by Talman (1968) and Varshalovich et al. (1988)). In terms of ultraspherical polynomials $C^{(\alpha)}_n$, defined as the coefficients of the expansion

$$(1 - 2xy + y^2)^{-\lambda} = \sum_{n=0}^{\infty} C^{\lambda}_N(y) x^n,$$

it can be written as

$$H_{jL}(\chi) = (2L)!! \sqrt{\frac{(2j+1)(2j-L)!}{(2j+L+1)!}} \times (\sin\chi)^L C^{(L+1)}_{2j-L}(\cos\chi)$$

The angle χ is determined by

$$\cos\chi = \frac{1 + \alpha^2 \cos\Delta\Phi\sqrt{1+\alpha^2}}{1+\alpha^2} \tag{18}$$

and is called a *collision* parameter defined both by the Stark parameter $\alpha = 3Z/2\tilde{b}\tilde{v}$ and by the polar angle $\Delta\Phi$ swept out by the internuclear vector $\boldsymbol{R}$ during the collision time τ_{coll}. Eq. (17) is capable of providing exact numerical results [19] even for large quantum numbers n, in contrast to previous expressions [17,18] where the number of terms to be summed increases

dramatically with n. Note that the capacity of the projectile to produce angular momentum changes is governed solely by the parameter χ, the argument of H_{jL} in Eq. (17). Since $\Delta\Phi$ varies with time t, expression (17) furnishes $P^{(n)}_{\ell'\ell}$ as a function of t and Stark parameter α, all absorbed within *collision* parameter χ.

It can be shown from (17) that both detailed balance $(2\ell+1)P^{(n)}_{\ell'\ell} = (2\ell'+1)P^{(n)}_{\ell\ell'}$ and probability conservation $\sum_{\ell'} P^{(n)}_{\ell'\ell} = 1$ are satisfied. It is important to note that the above solution (17) for $P^{(n)}_{\ell'\ell}$ is equivalent to the numerical solution that would, in principle, be obtained from the very large $(n^2 \times n^2)$ set of coupled differential equations resulting from closely-coupling all n^2 quantal $n\ell m$ states. Since the dipole interaction alone couples $\ell \to \ell \pm 1$ transitions, the sequence of transitions occurring during the collision time $\tau_{\rm coll} \approx b/v$ is then $\ell \rightleftharpoons (\ell+1) \rightleftharpoons (\ell+2) \rightleftharpoons \cdots \rightleftharpoons \ell'_{\rm max}$ and $\ell \rightleftharpoons (\ell-1) \rightleftharpoons (\ell-2) \rightleftharpoons \cdots \rightleftharpoons \ell'_{\rm min}$. This physical sequence is acknowledged theoretically by the exponential nature of the interaction evolution operator (13).

4.3. Transitions from $\ell = 0$

For the special case of zero initial angular momentum, the $6-j$ symbol is (formula (1) page 299 in [22])

$$\begin{Bmatrix} \ell' & 0 & L \\ j & j & j \end{Bmatrix} = (-1)^{\ell'+n+1} \frac{\delta_{\ell' L}}{\sqrt{n(2\ell'+1)}}$$

to give the transition probability for $0 \to \ell'$ transitions as

$$P^{(n)}_{\ell' 0}(\chi) = \frac{2\ell'+1}{n^2} H^2_{j\ell'}(\chi),$$

which is identical with the previous result of Kazansky and Ostrovsky [14]. Eq. (17) can then be written in the interesting form as

$$P^{(n)}_{\ell'\ell}(\chi) = n(2\ell'+1) \sum_{L=|\ell'-\ell|}^{n-1} \begin{Bmatrix} \ell' & \ell & L \\ j & j & j \end{Bmatrix}^2 P^{(n)}_{L0}(\chi)$$

Since the square of $6-j$ symbol is the probability of coupling three angular momenta, a physical interpretation may be given for the above formula. The Stark mixing transition may therefore be viewed as a multi-step process involving partial waves of angular momentum L.

4.4. Weak coupling approximation

The weak coupling limit of the exact quantal probability is obtained from the limit of (19) as $\alpha \to 0$. Then $\chi \approx 2\alpha + O(\alpha^3)$, $\cos\chi \to 1$ and $\sin\chi = 2\alpha$. The ultraspherical polynomial $C^{\lambda}_N(1) = (2\lambda + N - 1)/n$ so that (17) tends to

$$P^{(n)}_{\ell'\ell}(\alpha \to 0) = \frac{2\ell'+1}{n} \sum_{L=|\ell'-\ell|}^{n-1} (2L+1) \begin{Bmatrix} \ell' & \ell & L \\ j & j & j \end{Bmatrix}^2 \times \left[\frac{2^{2L} L!}{(2L+1)!} \sqrt{\frac{n(n+L)!}{(n-L-1)!}} \alpha^L \right]^2 \tag{19}$$

where $j = 2n+1$. This weak-coupling result allows all $\ell \to \ell'$ transitions. The leading term of the probability (19) varies as α^{2L}, with $L = |\ell - \ell'| = 1$ for optically allowed and $L = 2, 3, 4, \ldots$ for forbidden transitions. Since

$$\begin{Bmatrix} \ell \pm 1 & \ell & 1 \\ j & j & j \end{Bmatrix}^2 = \frac{(n^2 - \ell_>^2)\ell_>}{n(n^2-1)(4\ell_>^2 - 1)},$$

the dipole ($L = 1$) contribution to the weak-coupling probability (19) is

$$P^{D}_{n\ell \to n'\ell\pm 1} = 3Z^2 \frac{\ell_>}{2\ell+1} n^2 (n^2 - \ell_>^2) \left(\frac{a_0 v_0}{bv}\right)^2 = \frac{4}{3} \frac{\ell_>}{2\ell+1} n^2 (n^2 - \ell_>^2) \alpha^2 \tag{20}$$

which varies as α^2. This result (20) satisfies detailed balance and agrees with the Born limit (Section 6) for $\ell \to \ell \pm 1$ dipole transitions.

4.5. Integral cross-section

The integral cross-section for Stark mixing is

$$\sigma_{n\ell \to n\ell'} = 2\pi \int_0^\infty P^{(n)}_{\ell'\ell} b \, {\rm d}b = 4.5 Z^2 \pi a_n^2 \left(\frac{v_n}{v}\right)^2 \times \int_{\alpha_{\rm min}}^\infty P^{(n)}_{\ell'\ell}(\alpha, \Delta\Phi) \frac{{\rm d}\alpha}{\alpha^3} \tag{21}$$

A lower limit $\alpha_{\min}$ is imposed [17] in order to account for physical effects as quantum defects, spin-orbit coupling and Debye screening in a plasma, which depend, of course, on the specific problem considered. This prevents the well known logarithmic divergence which originates in (21) from the $\alpha \to 0$ weak coupling limit (20) of (17) for $\ell \to \ell \pm 1$ transitions. The cross-sections for optically forbidden transitions exhibit no such divergence.

5. Classical theory

5.1. Classical intrashell dynamics

In the presence of an electric field of intensity $\boldsymbol{\mathcal{E}}$, the angular momentum $\boldsymbol{L}$ changes at the rate

$$\frac{\mathrm{d}\boldsymbol{L}}{\mathrm{d}t} = -e\boldsymbol{r} \times \boldsymbol{\mathcal{E}}$$

The collision is adiabatic with respect to the electronic orbital motion, ($\omega_{\mathrm{R}} = \dot{\Phi} \ll \omega_n$), so that $\boldsymbol{\mathcal{E}}$ is constant over one period τ_n and the collision lasts over many ($\simeq$50) periods. The secular change of $\boldsymbol{L}$ during the collision is then the classical average

$$\frac{\mathrm{d}\boldsymbol{L}}{\mathrm{d}t} = \frac{\Delta \boldsymbol{L}}{\tau_n} = -\frac{e}{\tau_n}\int_{t-\tau_n/2}^{t+\tau_n/2} (\boldsymbol{r} \times \boldsymbol{\mathcal{E}})\,\mathrm{d}t' = -\left(\frac{3e}{2p_n}\right)\boldsymbol{\mathcal{E}}(t) \times \boldsymbol{A}(t)$$

over one orbital period τ_n. Although the vectors $\boldsymbol{L}$ and $\boldsymbol{A}$ change very little during each τ_n, consistent with the weak field approximation ($\omega_{\mathrm{S}} \ll \omega_n$), they do suffer significant change over many τ_n. The following set of coupled equations can then be deduced [8,20]

$$\frac{\mathrm{d}\boldsymbol{A}}{\mathrm{d}t} = -\boldsymbol{\omega}_{\mathrm{S}} \times \boldsymbol{L}, \qquad \frac{\mathrm{d}\boldsymbol{L}}{\mathrm{d}t} = -\boldsymbol{\omega}_{\mathrm{S}} \times \boldsymbol{A}$$

where $\boldsymbol{\omega}_{\mathrm{S}} = \alpha\dot{\Phi}\hat{R}$ varies with time. Under the substitution

$$\boldsymbol{M} = \frac{\boldsymbol{L} + \boldsymbol{A}}{2}, \qquad \boldsymbol{N} = \frac{\boldsymbol{L} - \boldsymbol{A}}{2} \tag{22}$$

the above set decouples to yield the set

$$\frac{\mathrm{d}\boldsymbol{M}}{\mathrm{d}\Phi} = -\alpha\hat{\boldsymbol{R}} \times \boldsymbol{M}, \qquad \frac{\mathrm{d}\boldsymbol{N}}{\mathrm{d}\Phi} = +\alpha\hat{\boldsymbol{R}} \times \boldsymbol{N} \tag{23}$$

of uncoupled equations. Since the averaged energy-change rate

$$\frac{\mathrm{d}E}{\mathrm{d}t} = \frac{\Delta E}{\tau_n} = -\frac{e}{\tau_n}\int_{t-\tau_n/2}^{t+\tau_n/2} \boldsymbol{\mathcal{E}} \cdot \dot{\boldsymbol{r}}\,\mathrm{d}t = -e\boldsymbol{\mathcal{E}}(t) \cdot \langle \dot{\boldsymbol{r}} \rangle \approx 0$$

there is no secular change to the Rydberg energy E. The magnitudes $M^2 = N^2 = (L^2 + A^2)/4 = n^2\hbar^2/4$ therefore remain constant throughout the collision. This set (23) can be solved exactly and solutions for $\boldsymbol{A}(t)$ and $\boldsymbol{L}(t)$ obtained [16,17] in terms of their initial values, α and $\Delta\Phi$.

5.2. Classical transition probability

The hypersurface in the $\{\boldsymbol{L}\} \otimes \{\boldsymbol{A}\}$ space on which the initial state is uniformly distributed is restricted by the constraints in Section 1 and has the volume:

$$\mathcal{V}_{n\ell} = \iint \delta(|\boldsymbol{L}| - \ell\hbar)\delta(|\boldsymbol{A}| - \hbar\sqrt{n^2 - \ell^2}) \times \delta(\boldsymbol{L} \cdot \boldsymbol{A})\,\mathrm{d}\boldsymbol{L}\,\mathrm{d}\boldsymbol{A} \tag{24}$$

which integrates to

$$\mathcal{V}_{n\ell} = 8\pi^2\ell\sqrt{n^2 - \ell^2}\hbar^2$$

Each point within this manifold evolves during the collision according to the above solutions for $\boldsymbol{A}(t)$ and $\boldsymbol{L}(t)$, so that only a fraction of possible initial states can have the final angular momentum ℓ' after the collision. Following the definition (24), the overlap volume of accessible $(\boldsymbol{L}, \boldsymbol{A})$ space which contains both initial and final states is

$$\mathcal{V}_{n\ell\ell'} = \iint \delta(|\boldsymbol{L}| - \ell\hbar)\delta(|\boldsymbol{L}'| - \ell'\hbar) \times \delta(|\boldsymbol{A}| - \hbar\sqrt{n^2 - \ell^2})\delta(\boldsymbol{L} \cdot \boldsymbol{A})\,\mathrm{d}\boldsymbol{L}\,\mathrm{d}\boldsymbol{A} \tag{25}$$

The transition probability is defined as the ratio

$$P^{(n)}_{\ell'\ell} = \frac{\mathcal{V}_{n\ell\ell'}}{\mathcal{V}_{n\ell}} \tag{26}$$

of phase space volumes. The classical transition probability is therefore defined in this new $(\boldsymbol{A}, \boldsymbol{L})$ phase

space, designed to exploit the dynamical symmetry, as the normalized volume of phase space accessible to both initial and final states. This overlap volume is the volume occupied by those final states which originate from the initial states and is illustrated in Fig. 2.

Upon integrating (25), the classical transition probability obtained [16,17] from (26) is written as the following analytic expression

$$P^{(n)}_{\ell'\ell}(\chi) = \frac{2(\ell'/n)}{\pi\hbar|\sin\chi|} \begin{cases} 0, & \text{if } |\sin\chi| < |\sin(\eta_1-\eta_2)| \\ \dfrac{K\{[\sin^2(\eta_1+\eta_2)-\sin^2(\eta_1-\eta_2)]/\sin^2\chi-\sin^2(\eta_1-\eta_2)\}}{\sqrt{\sin^2\chi-\sin^2(\eta_1-\eta_2)}}, & \text{if } |\sin\chi| > |\sin(\eta_1+\eta_2)| \\ \dfrac{K\{[\sin^2\chi-\sin^2(\eta_1-\eta_2)]/\sin^2(\eta_1+\eta_2)-\sin^2(\eta_1-\eta_2)\}}{\sqrt{\sin^2(\eta_1+\eta_2)-\sin^2(\eta_1-\eta_2)}}, & \text{if } |\sin\chi| < |\sin(\eta_1+\eta_2)|. \end{cases} \tag{27}$$

The classical probability is a function of the same collisional parameter χ basic to the quantal result (17) and given by (18), and also of the angles η_1 and η_2 determined by

$$\cos\eta_1 \equiv \frac{\ell}{n} = \epsilon \quad \text{and} \quad \cos\eta_2 \equiv \frac{\ell'}{n} = \epsilon', \tag{28}$$

the initial and final state ratios $\epsilon = \ell/n$ and $\epsilon' = \ell'/n$. Note that the eccentricities $\epsilon_{i,f}$ of the initial and final classical Kepler orbits are $\sin\eta_{1,2}$. The collision parameter χ increases monotonically with the Stark parameter $\alpha = 3Z/2\tilde{b}\tilde{v}$ as

$$\chi \approx 2\alpha \sin\left(\frac{\Delta\Phi}{2}\right) + \mathcal{O}(\alpha^3)$$

The transition probability $P^{(n)}_{\ell'\ell}(\chi)$ can be also interpreted as the distribution of final states with angular momentum ℓ' which originate from one initial state of angular momentum ℓ and result from collision with a charged projectile. The probability (27) satisfies detailed balance $2\ell P_{\ell'\ell} = 2\ell' P_{\ell\ell'}$, where 2ℓ is the classical weight of the state $n\ell$. Moreover, the classical limit of the full quantal probability (17) can be directly and easily obtained to provide a result identical with (27).

6. Results

6.1. Quantal–classical convergence

The classical function $nP^{(n)}_{\epsilon' n,\epsilon n}(\chi)$ of (27) is independent of n. Such universal functions can be uncovered within classical treatments, in general, and this feature will be exploited, to explore the rapid convergence of the quantal results onto the classical frame as n is increased. Fig. 3 illustrates the rapid convergence with n for all transitions from a given initial ℓ at a given collision parameter $\chi \sim 1/bv$. Fig. 4 demonstrates the rapid convergence with n for a specific $\ell \to \ell'$ transition over all χ. The quantal results oscillate in general about the universal classical frame. The structure of the classical frames of Figs. 3 and 4 can be explained in terms of two distinct regions within the classical accessible region, and two classical inaccessible regions. This structure remains obscured within the quantal results.

6.2. Structure

Representative probabilities as a function of ℓ' are presented in Fig. 5 for the $n = 28, \ell = 18 \to 28, \ell'$ transitions in atomic hydrogen. The increasing values of $\chi \sim 1/bv \sim \tau_{\text{coll}}/b^2$ corresponds to a series of collisions either at fixed impact parameter b and decreasing v, or vice-versa. Increasing χ therefore corresponds to lengthening the duration of a collision at fixed b. Since the dipole interaction couples $\ell \to \ell \pm 1$ states, the sequence of transitions which occur during the time τ_c of collision is then $\ell \rightleftharpoons (\ell-1) \rightleftharpoons (\ell-2) \rightleftharpoons \cdots \rightleftharpoons \ell'_{\text{min}}$ and $\ell \rightleftharpoons (\ell+1) \rightleftharpoons (\ell+2) \rightleftharpoons \cdots \rightleftharpoons \ell'_{\text{max}}$. For the shorter collision times τ_c,

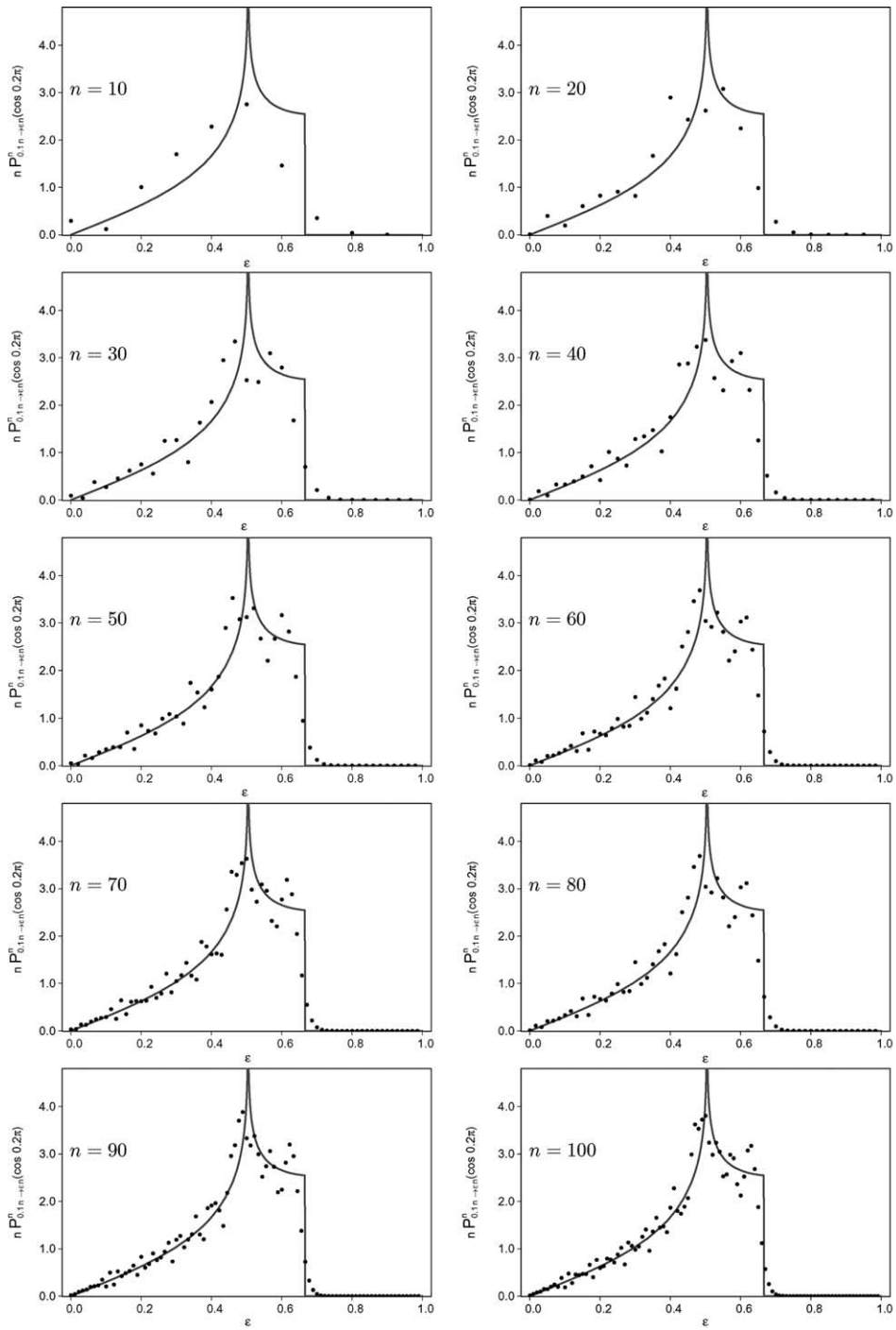

Fig. 3. Plots of the scaled transition probability $nP^{(n)}_{\ell\to\epsilon n}(\chi)$ as a function of the ratio $\epsilon = \ell'/n$ illustrating, as n increases, the convergence of the exact quantal results (blue dots) onto the fixed classical framework (red line), at constant values of the ratios $\ell/n = 0.1$ and collision parameter $\chi = 0.2\pi$.

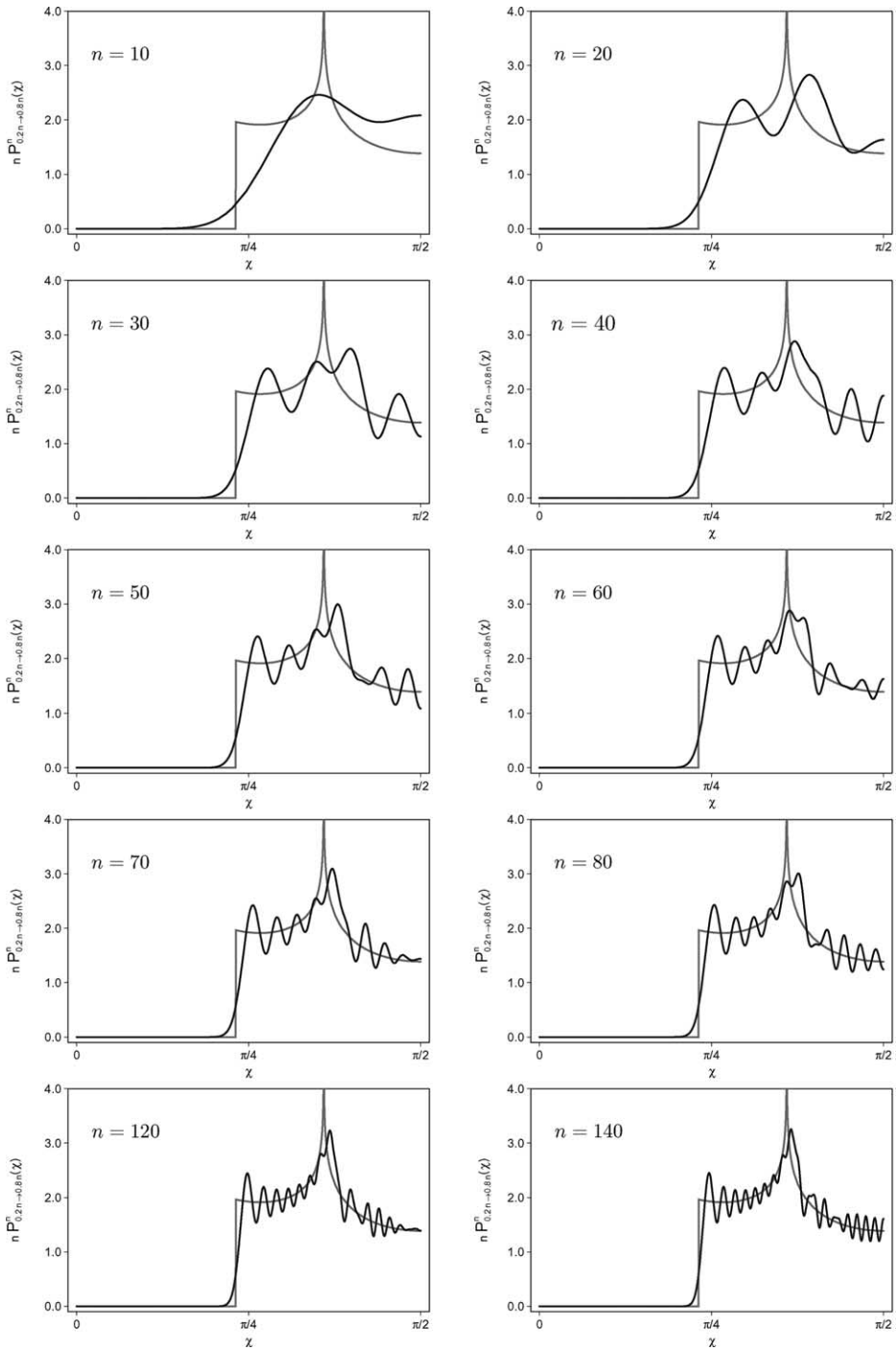

Fig. 4. Plots of the scaled transition probability $nP^{(n)}_{\epsilon n\to\epsilon' n}(\chi)$ as a function of collision parameter χ illustrating, as n increases, the convergence of the exact quantal result (blue line) onto the fixed classical framework (red line), for constant values of the ratios $\epsilon = \ell/n$ and $\epsilon' = \ell'/n$.

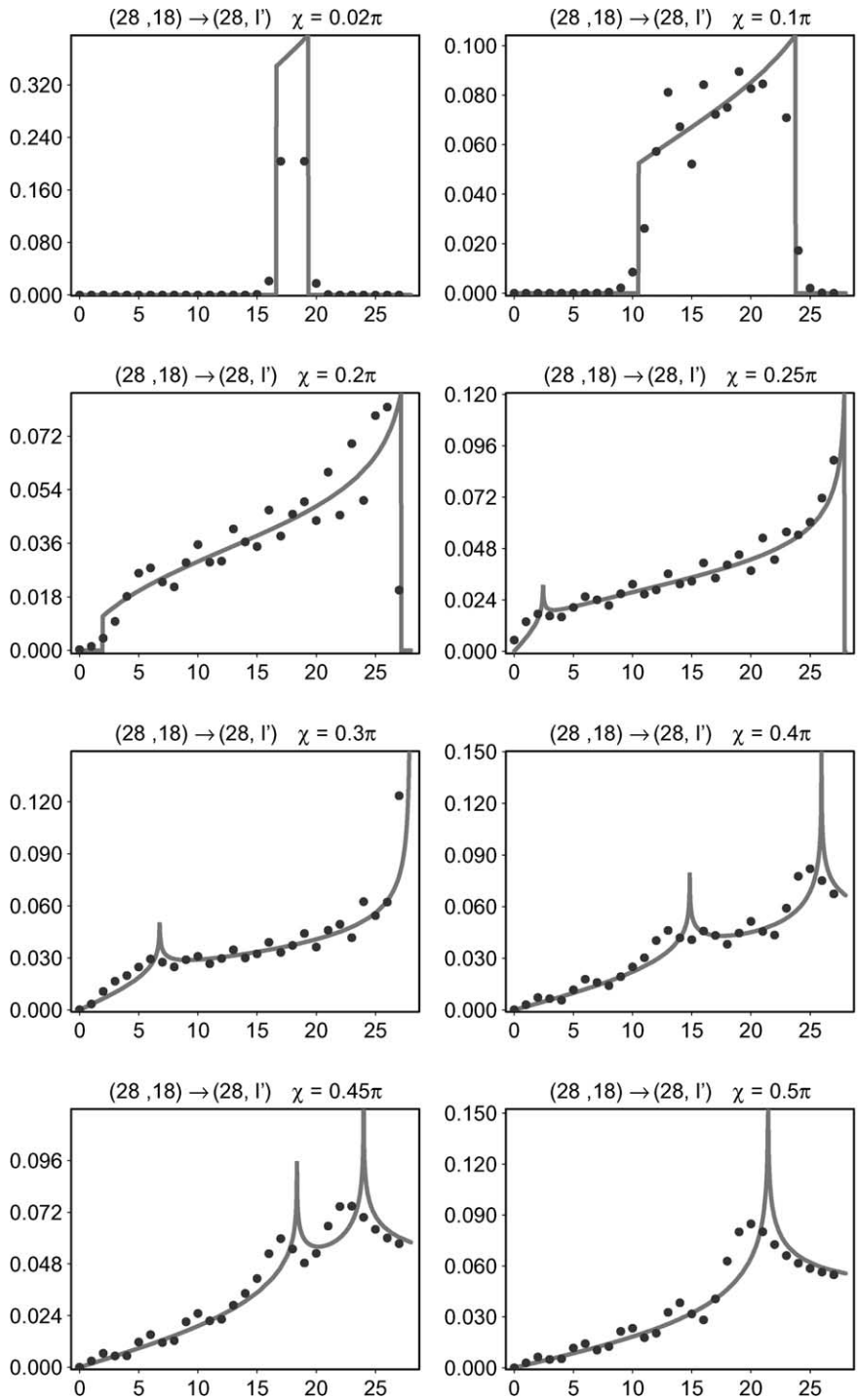

Fig. 5. Quantal and classical transition probabilities $P^{(n)}_{\ell'\ell}(\chi)$ for Stark mixing from initial $\ell = 11$ to final ℓ' states within the $n = 28$ energy shell at specific values of the collision parameter χ.

corresponding to small χ, $\ell'_{\min}$ and $\ell'_{\max}$ do remain well within the boundary values 0 and $n-1$ of the angular momentum. There is insufficient time to sequentially access the highest or lowest values of ℓ' during the collision. Steps then appear in the classical structure. Within the classical inaccessible regions, the quantal results exhibit the characteristic exponentially decreasing and increasing variation. When the extreme limits, $\ell' = 0$ and $\ell' = n-1$, of angular momentum can be accessed during the collision, then these limits act, in turn, as additional sources which then proceed to populate the $\ell' = 1, 2, \ldots$ and $\ell = n-2, n-3, \ldots$ states from below and above, throughout the duration of the collision. The classical probabilities then exhibit two distinct cusps arising from these secondary sources. These cusps merge into one as the collision duration time continues to increase with increasing values of the collision parameter χ. The ℓ'-locations of the classical steps and cusps in (27) are determined by the solutions of $|\sin(\eta_1 - \eta_2)| = |\sin\chi|$ and $|\sin(\eta_1 + \eta_2)| = |\sin\chi|$, respectively. The structure in Fig. 3 (which corresponds to one of the structures in Fig. 5) can therefore be physically explained.

A map of the various classical zones in the plane of reduced initial and final angular momenta $(\ell/n, \ell'/n)$ is displayed in Fig. 6 for the four values, $\alpha = 0.2$, 0.4, 0.6 and 0.8 of the Stark parameter and for $\Delta\Phi = -\pi$, appropriate to an undeflected classical path. Quantities

$$\mathcal{A} = |\sin\chi| - |\sin(\eta_1 + \eta_2)| \tag{29}$$

and

$$\mathcal{B} = |\sin\chi| - |\sin(\eta_1 - \eta_2)| \tag{30}$$

are useful to describe the various possibilities. In the central region $\mathcal{A}$ is negative and $\mathcal{B}$ is positive. Within the lower left and upper right corners both $\mathcal{B}$ and $\mathcal{A}$ are positive. The transition is classically forbidden where $\mathcal{B} < 0$ in the upper left and lower right corners (gray zones). Across the separatrix (dotted line) which separates the classical inacessible/accessible regions, the

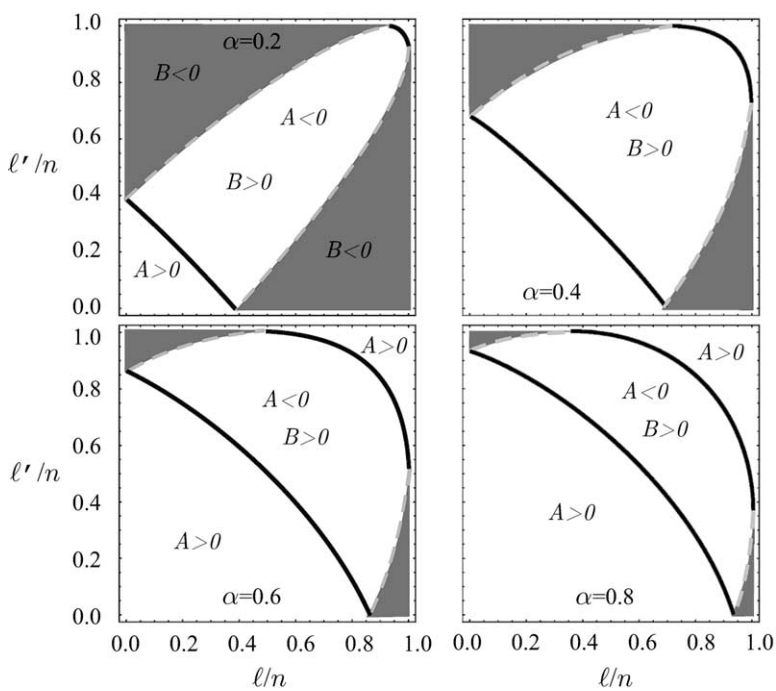

Fig. 6. Contour plots of the solutions of $\mathcal{A} = 0$ (solid line) and $\mathcal{B} = 0$ (dotted line) for various values of α. In gray zones $\mathcal{B} < 0$ and the transition is classically forbidden.

transition probability jumps from zero (in the gray zone) to some finite value (in the central zone). Along the solid line, for which $\mathcal{A} = 0$, the transition probability has a logarithmic (cusp) singularity. As $\alpha \to 0$, the two inaccessible regions (where $\mathcal{B} < 0$) broaden until the central region with $\mathcal{B} > 0$ and $\mathcal{A} < 0$ becomes an elongated line strip lying along the diagonal $\ell = \ell'$. Only elastic and dipole transitions are therefore permitted in the limit $\alpha \to 0$. As α increases to unity the classically forbidden zones diminish and the collision becomes more and more effective in its ability to induce larger angular momentum changes. By appeal to Fig. 6, the structures in Figs. 3 and 5 can be fully explained.

Fig. 7 presents maps corresponding to Fig. 6. The same characteristic regions are now displayed in the plane of final reduced angular momentum ℓ'/n and the Stark parameter α for four values of the initial reduced angular momentum $\ell/n = 0.071$, 0.36, 0.64, and 0.93. Again, the classically forbidden regions (gray zones), correspond to the condition $\mathcal{B} < 0$, in the left upper and lower corners. The elastic $\ell' = \ell$ transitions are always possible, even when $\alpha \to 0$. Again, along the solid ($\mathcal{A} = 0$) and dotted ($\mathcal{B} = 0$) lines, the transition probabilities have cusp and step singularities. When α (or χ) increases the span of possible final angular momentum, for given angular momentum, increases. Large (small) angular momentum transfer is only possible for collisions with large (small) Stark parameters. This behavior is exhibited in the quantal/classical probabilities of Fig. 8 as a function of collision parameter χ. The structure in Fig. 4 corresponds to one of the structures in Fig. 8. In summary, both Figs. 6 and 7 are key to interpretation of Figs. 5 and 8 for the variation of the probabilities $P_{\ell'\ell}(\alpha)$ with both ℓ' and χ, respectively.

6.3. Quantal–classical correspondence

This is illustrated by Fig. 9 where the quantal probabilities are greatest in the vicinity of the classical cusp solid lines and exponentially decay as they transverse

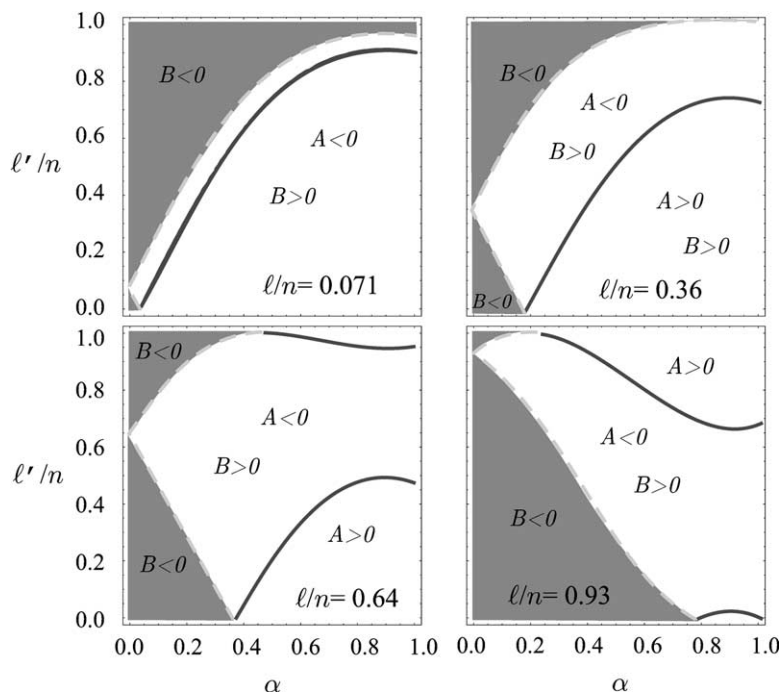

Fig. 7. Contour plots of the solutions of $\mathcal{A} = 0$ (solid line) and $\mathcal{B} = 0$ (dotted line) for various values of ℓ. In gray zones $\mathcal{B} < 0$ and the transition is classically forbidden.

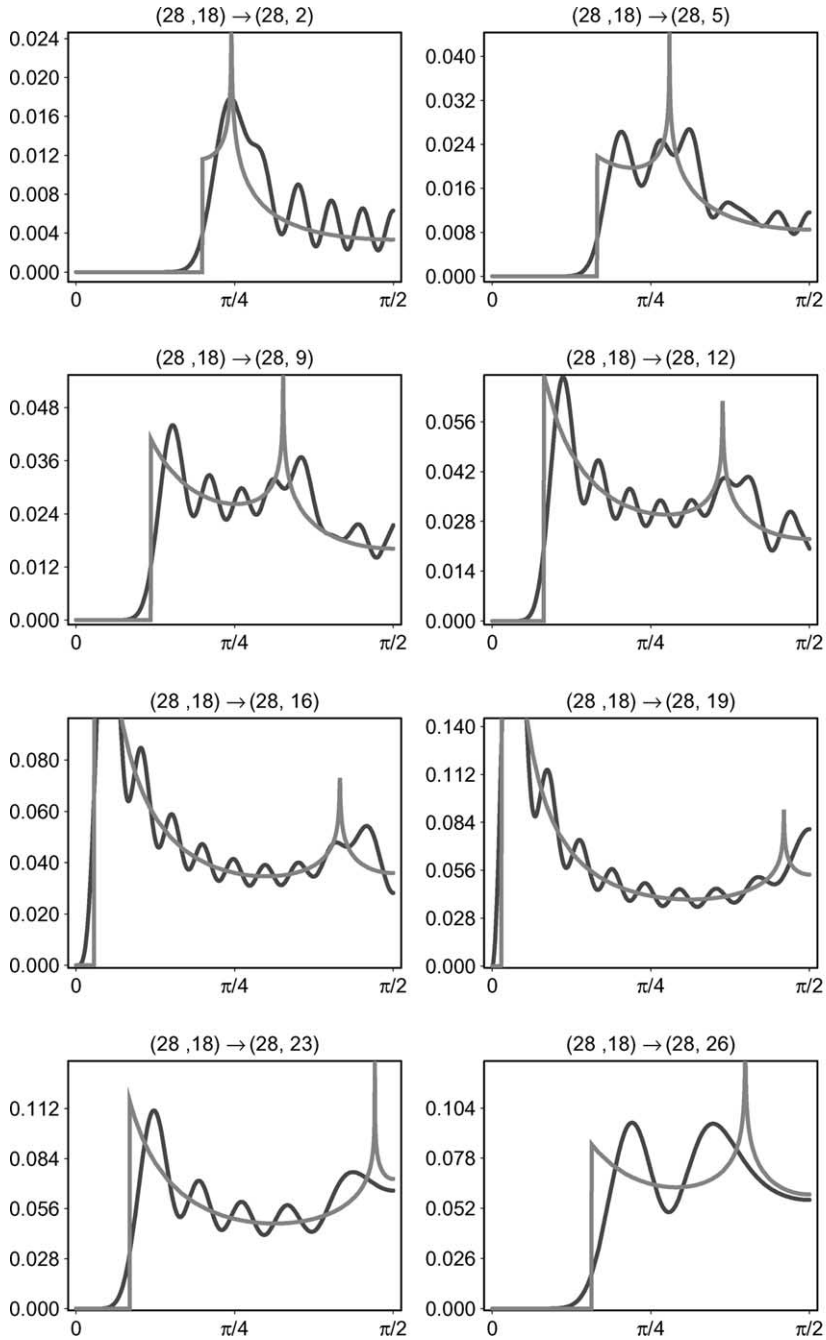

Fig. 8. Quantal and classical probabilities $P^{(n)}_{\ell'\ell}(\chi)$ for specific $\ell \rightarrow \ell'$ Stark mixing transitions within the $n = 28$ energy shell as a function of collision parameter χ.

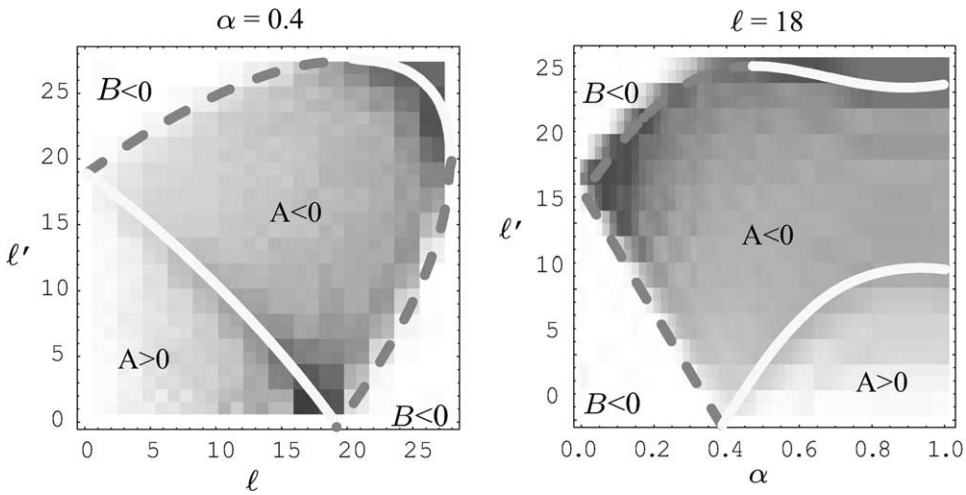

Fig. 9. Quantal–classical correspondence: variation with ℓ, ℓ' and Stark parameter α of quantal probabilities over the classical accessible and inaccessible regions. The higher probabilities (darker regions) are confined to the classical cusp (solid line) regions while the smaller exponentially decreasing probabilities are apparent in the classical inaccessible (dashed line) regions.

past the classical inaccessible (dashed line) regions. Figs. 5 and 8 are obtained from various cuts through Fig. 9.

7. Born limit

In the limit of weak coupling at all collision energies, the Born approximation

$$P^{\mathrm{B}}_{\ell\to\ell'} = \frac{1}{\hbar^2}\frac{1}{2\ell+1}\sum_{m,m'}\left|\int_{-\infty}^{\infty} V_i\, f[R(t)]\mathrm{e}^{i\omega_{\mathrm{if}}t}\,\mathrm{d}t\right|^2$$

for the probability of $\ell \to \ell' = \ell \pm 1$ transitions, which involve an energy defect $\epsilon_{\mathrm{fi}} = \hbar\omega_{\mathrm{fi}}$, yields

$$P^{\mathrm{B}}_{n\ell\to n'\ell'} = \left(\frac{2Ze^2\omega_{\mathrm{fi}}}{\hbar v^2}\right)^2 \frac{1}{2\ell+1} \times \sum_{m,m'}\left[|y^{n'\ell'm'}_{n\ell m}|^2 K_0^2\left(\frac{\omega_{\mathrm{fi}}b}{v}\right) + |z^{n'\ell'm'}_{n\ell m}|^2 K_1^2\left(\frac{\omega_{\mathrm{fi}}b}{v}\right)\right] \quad (31)$$

in terms of the y and z components of the dipole matrix element, $\langle\phi_{n'\ell'm'}|\boldsymbol{r}|\phi_{n\ell m}\rangle$, and the modified Bessel functions $K_{0,1}$. The collision takes place in the YZ-plane of Fig. 1. For atomic hydrogen, $\phi_{n\ell m} = R_{n\ell}Y_{\ell m}(\hat{r})$ so that $\sum_{m,m'}|y^{n'\ell\pm1m'}_{n\ell m}|^2 = (\ell_>/3)R^2_{n\ell,n'\ell\pm1}$ with $m' = m \pm 1$ and $\sum_{m,m'}|z^{n'\ell'm'}_{n\ell m}|^2 = (\ell_>/3)R^2_{n\ell,n'\ell\pm1}$, with $m = m'$. The dipole radial matrix element $R_{n\ell,n'\ell'}$ involving the radial wavefunctions $R_{n\ell}$ is $\int_0^\infty R_{n\ell}R_{n'\ell'}r^3\,\mathrm{d}r$. Hence,

$$\begin{aligned} P^{\mathrm{B}}_{n\ell\to n'\ell\pm1} &= 4Z^2\left(\frac{v_0}{v}\right)^4\left(\frac{\epsilon_{\mathrm{fi}}}{\epsilon_0}\right)^2\frac{\ell_>}{3(2\ell+1)} \times\left(\frac{R_{n\ell,n'\ell\pm1}}{a_0}\right)^2[K_0^2(\beta)+K_1^2(\beta)] \\ &= 4Z^2\left(\frac{a_0v_0}{bv}\right)^2\frac{\ell_>}{3(2\ell+1)}\left(\frac{R_{n\ell,n'\ell\pm1}}{a_0}\right)^2 \times\beta^2[K_0^2(\beta)+K_1^2(\beta)] \end{aligned} \quad (32)$$

where a_0, v_0 and ϵ_0 are atomic units and the parameter β is $\omega_{\mathrm{fi}}b/v \sim \omega_{\mathrm{fi}}/\omega_{\mathrm{coll}} \sim \tau_{\mathrm{coll}}/\tau_{\mathrm{tran}}$, the ratio of the collision time to the time τ_{tran} for the transition. When convenient, $P^{\mathrm{B}}_{n\ell\to n'\ell\pm1}$ may also be expressed in terms of the oscillator strength

$$f_{n\ell,n'\ell\pm1} = \frac{2\ell_>}{3(2\ell+1)}\left(\frac{\epsilon_{\mathrm{fi}}}{\epsilon_0}\right)\left(\frac{R_{n\ell,n'\ell\pm1}}{a_0}\right)^2$$

For Stark mixing collisions, $n = n'$, $\beta^2[K_0^2(\beta) + K_1^2(\beta)] = 1$ and $R^2_{n\ell,n'\ell\pm1} = (9n^2/4)(n^2 - \ell_>^2)a_0^2$, so that (32) yields

$$P^{\mathrm{B}}_{n\ell\to n'\ell\pm1} = 3Z^2\frac{\ell_>}{2\ell+1}n^2(n^2-\ell_>^2)\left(\frac{a_0v_0}{bv}\right)^2 = \frac{4}{3}\frac{\ell_>}{2\ell+1}n^2(n^2-\ell_>^2)\alpha^2 \quad (33)$$

which is identical, as expected, with the weak-coupling dipole contribution (32), the first term ($L = 1$) of (19).

8. Rydberg states with quantum defects

Rydberg atoms and molecules have quantum defects only for states with core penetrating electron orbits i.e., those with $\ell = 0$–2. These low-ℓ Rydberg wavefunctions, which are assumed known, are expanded here in terms of a hydrogenic basis set $|n\ell m\rangle$ as,

$$|RyN\ell m\rangle = \sum\int_n w_n^{(N\ell)}|n\ell m\rangle$$

and the amplitudes $w_n^{(N\ell)}$ determined. There is a small energy defect $\epsilon_{fi} = \hbar\omega_{fi}$ involved in transitions from low ℓ.

In order to account approximately for the probability of small energy transfer and by analogy with Section 7, it can be shown that the Stark Mixing quantal transition probability (17) becomes modified to

$$P_{N\ell\to N'\ell'} = (2\ell'+1)\sum_L(2L+1) \times\left[\sum\int_n\frac{(-1)^n}{\sqrt{n}}w_n^{(N'\ell')}w_n^{(N\ell)} \times\begin{Bmatrix}\ell' & \ell & L\\ j & j & j\end{Bmatrix}H_{jL}(\chi)\right]^2\left(\frac{\omega_{fi}b}{v}\right)^2 \times\left[K_0^2\left(\frac{\omega_{fi}b}{v}\right)+K_1^2(\omega_{fi}b/v)\right] \quad (34)$$

The weak coupling limit of (34) is (32). While the present theory has been developed for individual $n\ell \to n\ell'$ transitions in Rydberg atoms, the only available measurements of Stark Mixing are those of Sun and MacAdam [6] who provided normalized measured fractional populations for Na(28d) → Na(28f), Na(28g + 28h), Na(28f + 28g + 28h) transitions in Na^+–Na(28d) collisions. Fig. 10 illustrates the general agreement between the measurements and our corresponding calculations based on (34).

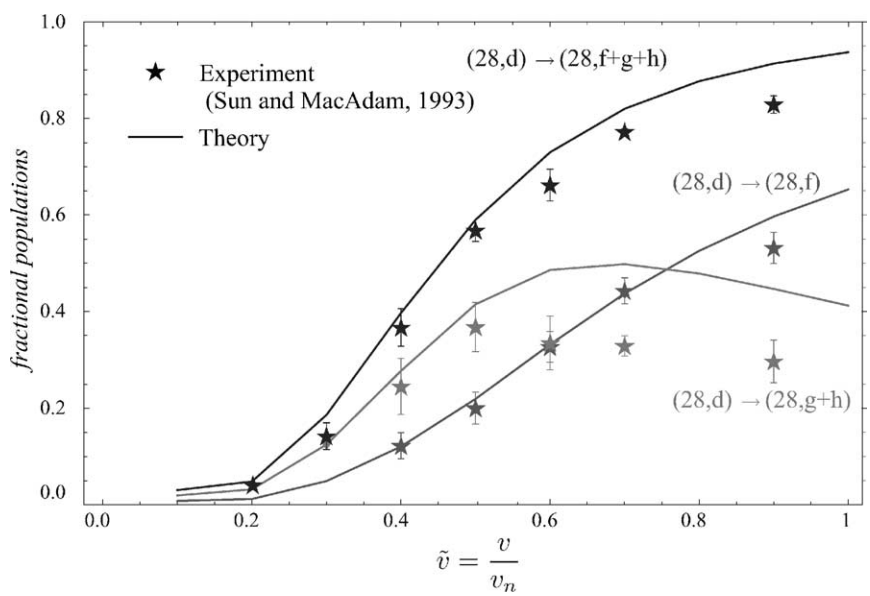

Fig. 10. Fractional populations for Na(28d) → Na(28f), Na(28g + 28h), Na(28f + 28g + 28h) transitions.

9. Summary and conclusions

We have presented here a case study of collisional Stark mixing within the full array of $n\ell \rightarrow n\ell'$ transitions induced by ion–Rydberg atom collisions at ultralow energies. The inherent group dynamic symmetry permits development of exact solution in both quantal and classical formulations. The solutions are presented in compact form reflecting the mathematical beauty of the problem as well as pragmatic value. The quantal (17) and classical (27) results complement each other. The leading (dipole) term (20) of the weak coupling limit (19) is identical, as expected, with the Born result (33) for $\ell \rightarrow \ell \pm 1$ dipole transitions alone. A universal classical probability $nP^{(n)}_{\epsilon' n,\epsilon n}(\chi)$ was deduced which allowed illustration of rapid convergence of the quantal to the classical results with increasing principal quantum number n. The structure exhibited in the variation of $P^{(n)}_{\ell'\ell}$ with ℓ' is explained and a quantal–classical correspondence is manifest. A modified theory (34) was then provided to acknowledge quantum defects (low ℓ) in non-hydrogenic systems. Essential agreement is obtained with measurements [6]. Collisional Stark mixing at ultralow energies is probably one of the last remaining problems in collision physics capable of exact theoretical solution.

Acknowledgements

This research has been supported by AFOSR Grant No. 49620-99-1-0277 and NSF Grant No. 01-00890.

References

[1] M.R. Flannery, D. Vrinceanu, in: E. Oks, M.S. Pindzola (Eds.) Atomic Processes in Plasmas, 11th APS Topical Conference, AIP Press, New York, 1998, p. 317.
[2] F. Merkt, R.N. Zare, J. Phys. Chem. 101 (1994) 3495.
[3] S.R. Lundeen, in: J.B.A. Michell, S.L. Guberman (Eds.), Dissociative Recombination: Theory, Experiment, and Applications, World Scientific, Singapore, 1989, p. 182.
[4] R.J.T. Gougousi, M.F. Golde, Int. J. Mass. Spectrom. Ion Process. 149/150 (1995) 131.
[5] M.R. Flannery, D. Vrinceanu, in: S.L. Guberman (Ed.), Dissociative Recombination: Theory, Experiment, and Applications, Kluwer Academic/Plenum Press, Singapore, 2002.
[6] X. Sun, K.B. MacAdam, Phys. Rev. A 47 (1993) 3913.
[7] R.M. Pengelly, M.J. Seaton, Monthly Notices Roy. Astronom. Soc. 127 (1964) 165.
[8] I.C. Percival, D. Richards, J. Phys. B 12 (1979) 2051.
[9] Y.N. Demkov, B.S. Monozon, V.N. Ostrovskii, Sov. Phys. JETP 30 (1970) 775.
[10] I.L. Beigman, V.S. Lebedev, Phys. Rep. 250 (1995) 95.
[11] P. Bellomo, D. Farrelly, T. Uzer, J. Chem. Phys 107 (1995) 2499.
[12] A.K. Kazansky, V.N. Ostrovsky, Phys. Rev. A 53 (1995) 1811.
[13] A.K. Kazansky, V.N. Ostrovsky, J. Phys. B 29 (1996) 3651.
[14] A.K. Kazansky, V.N. Ostrovsky, Phys. Rev. Lett. 77 (1996) 3094.
[15] A.K. Kazansky, V.N. Ostrovsky, Sov. Phys. JETP 83 (1996) 1095.
[16] D. Vrinceanu, M.R. Flannery, Phys. Rev. Lett. 85 (2000) 4880.
[17] D. Vrinceanu, M.R. Flannery, Phys. Rev. A 63 (2001) 32701.
[18] D. Vrinceanu, M.R. Flannery, J. Phys. B 33 (2000) 721.
[19] D. Vrinceanu, M.R. Flannery, J. Phys. B 34 (2001) 1.
[20] M. Born, The Mechanics of the Atom, Ungar, New York, 1960, p. 235.
[21] W. Pauli, Z. Phys. 36 (1926) 336.
[22] D.A. Varshalovich, A.N. Moskalev, V.K. Khersonskii, Quantum theory of angular momentum, World Scientific, Singapore, 1988, p. 260.